ACS APPLIED MATERIALS & INTERFACES

Research Article

www.acsami.org

Size-Dependent Two-Photon Excitation Photoluminescence Enhancement in Coupled Noble-Metal Nanoparticles

Fei Han,[§,†,‡] Zhenping Guan,[†,§] Teck Soon Tan,[†] and Qing-Hua Xu*[,†,‡]

[†]Department of Chemistry, National University of Singapore, Singapore 117543

[‡]NUSNNI-Nanocore, National University of Singapore, Singapore 117576

Supporting Information

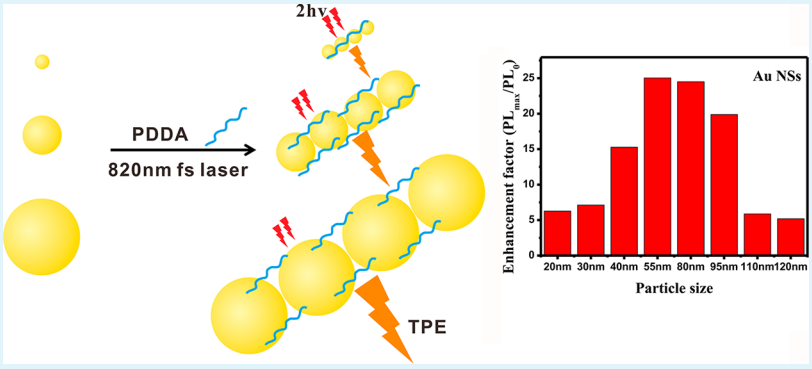

ABSTRACT: Plasmon coupling is known to enhance the two-photon excitation photoluminescence of metal nanoparticles significantly. Here, Au and Ag nanospheres of different sizes were prepared to systematically investigate the effects of particle size on plasmon coupling enhanced two-photon excitation photoluminescence. An oppositely charged polyelectrolyte, poly(diallyldimethylammonium chloride) (PDDA), was used to induce the coupling of Au and Ag nanospheres. The two-photon excitation photoluminescence enhancement factor was found to first increase and then decrease with the increasing particle size for both Au and Ag nanospheres. Optimum enhancement factors of 25-fold and 14-fold were obtained for coupled 55-nm Au nanospheres and 50-nm Ag nanospheres, respectively. The coupled Au and Ag nanospheres displayed two-photon action cross sections of up to 9×10^4 GM per particle (where 1 GM = 10^{-50} cm^4 s/photon). Similar to Ag nanoparticles, Au nanoparticles also displayed large coupling induced enhancement of two-photon excitation photoluminescence. Considering their excellent biocompatibility, high inertness, and easy preparation, Au nanoparticles are expected to find many new applications in two-photon biosensing and bioimaging.

KEYWORDS: *metal nanoparticles, plasmon resonance, two-photon excitation photoluminescence, size dependence, fluorescence enhancement, multiphoton excitation*

INTRODUCTION

Metal nanoparticles (NPs), such as Au and Ag, have found wide applications in various fields such as biosensing,[1] bioimaging,[2−5] electronics, and nonlinear optics,[6−9] because of their unique optical properties known as surface plasmon resonance (SPR). SPR arises from the collective oscillation of conduction band electrons and is sensitive to size, shape, and the surrounding medium environment of the metal NPs.[10−14] In addition, SPR can also be tuned by plasmon coupling of closely spaced metal NPs. The plasmon coupling can lead to red-shifted SPR bands and dramatically enhanced local electrical fields within the gap region.[15] The intense local field enhancement has been widely utilized to amplify the fluorescence, surface-enhanced Raman scattering (SERS), second-harmonic generation (SHG), and two-photon excitation photoluminescence (TPPL) properties of various materials.[2,16−25]

Two-photon excitation is important for many applications such as bioimaging, sensing, and phototherapy. Two-photon excitation based applications have many unique advantages over the traditional one-photon counterparts, such as three-dimensional (3D) selectivity, reduced photobleaching, and deep penetration into biological tissues.[26−28] TPPL from metal NPs is initiated by the excitation of electrons from the d-valence band to the sp-conduction band via two-photon absorption, followed by intraband scattering relaxation of the excited electron to the states near the Fermi surface before electrons and holes recombine radiatively.[19,29,30] Au and Ag NPs are generally considered to be nonfluorescent, because of their low quantum efficiency. The emission quantum efficiency of Au and Ag nanospheres were reported to be on the magnitude of 10^{-6}

Received: June 21, 2012
Accepted: August 14, 2012
Published: August 14, 2012

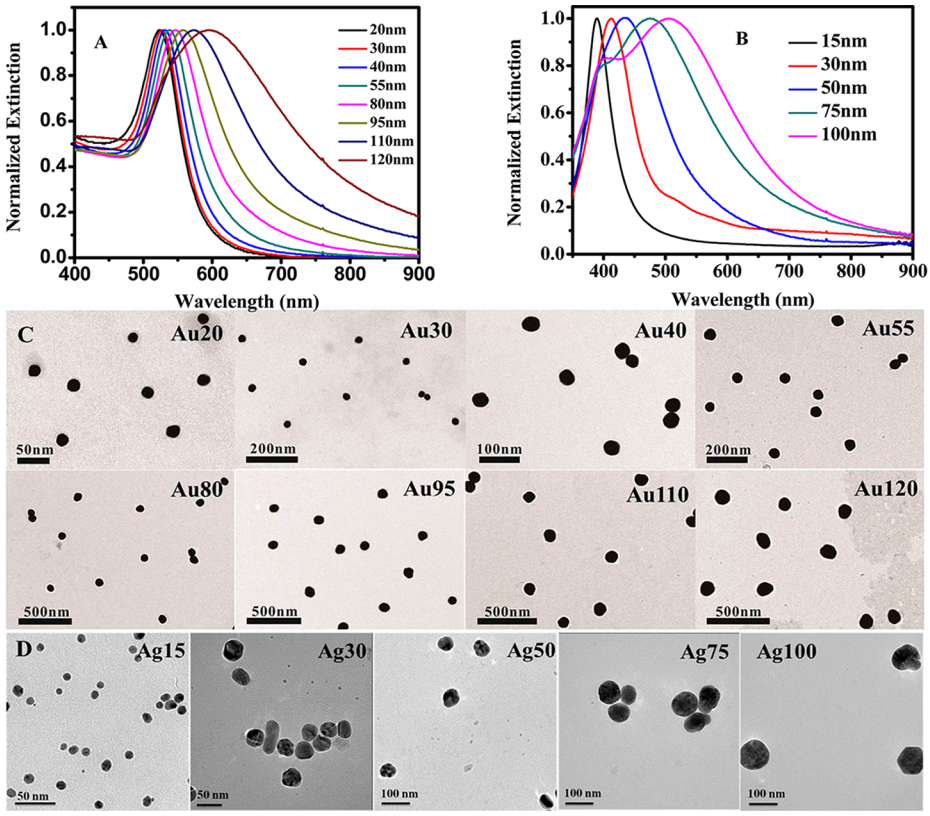

Figure 1. (A, B) Normalized extinction spectra and (C, D) TEM images of isolated Au NSs (panels A and C) and Ag NSs (panels B and D) of different sizes.

and 10^{-3}, respectively.[13,31] Although they are poor light emitters under one-photon excitation, Au and Ag nanorods, and coupled Au or Ag nanostructures were found to exhibit strong emission under two-photon excitation.[32,33] The longitudinal SPR band of these nanostructures provides enhanced local field as well as an intermediate state, which enhances two-photon excitation processes. These longitudinal plasmon modes are located in the near-IR region, coincident with the biological transparency window, which makes metal NPs attractive agents for in vivo biosensing, bioimaging, and phototherapy.[2−5,33,34]

Our group has previously reported significantly enhanced TPPL in coupled Ag NPs. The enhancement was ascribed to enhanced two-photon excitation, owing to formation of a longitudinal plasmon mode and enhanced local field at the excitation wavelength. The plasmon-coupling-enhanced TPPL of Ag NPs was further utilized to develop a new two-photon sensing platform for mercury detection with improved sensitivity and selectivity compared to the conventional colorimetric method.[34] Compared to Ag NPs, Au NPs are more attractive for biological applications, because of their low cytotoxicity and high inertness to the biological environment. In our previous work, 13-nm Au nanospheres (NSs) displayed much lower coupling-induced enhancement, compared to that of 37-nm Ag NSs.[32] Previous single-particle scattering studies revealed that local field enhancement was strongly dependent on the particle size and interparticle spacing.[35,36] Herein, we systematically investigated the influence of particle size on the coupling-induced TPPL enhancement. Au NSs of eight different sizes (from 20 nm to 120 nm) and Ag NSs of five different sizes (from 15 nm to 100 nm) were prepared to investigate the particle-size-dependent enhancement effects. A positively charged polyelectrolyte, poly(diallyldimethylammonium chloride) (PDDA), was used to induce the coupling of negatively charged Au and Ag NSs. The results show that Au NPs displayed similar TPPL enhancement magnitude as Ag NPs. These studies are expected to provide useful insight on improving TPPL enhancement of metal NPs and their practical applications such as bioimaging and sensing.

EXPERIMENTAL SECTION

Materials. Gold(III) chloride trihydrate ($HAuCl_4 \cdot 3H_2O$, 99.9%), silver nitrate ($AgNO_3$, 99.9%), poly(diallyldimethylammonium chloride) (PDDA, M_w 400 000−500 000, 20 wt % in H_2O) were purchased from Sigma−Aldrich. Trisodium citrate dihydrate (99%) was purchased from Fluka. Ascorbic acid was purchased from Alfa Aesar. All regents were analytical grade and used as received without further purification. All aqueous solutions were prepared in deionized water.

Preparation of Au Nanospheres (Au NSs). Au NSs were prepared following a kinetically controlled seeded growth strategy via reduction of $HAuCl_4$ by trisodium citrate.[37] Briefly, 2.2 mM trisodium citrate solution (37.5 mL) was heated to boiling under vigorous stirring, followed by the injection of a 25 mM $HAuCl_4$ solution (250 μL). The gold seeds were obtained when the solution color turned wine-red. Once the seed solution was cooled to 90 °C, 0.25 mL of 25 mM $HAuCl_4$ solution was injected and the reaction was allowed to proceed for 30 min. This step was repeated twice. The solution was then diluted by adding 13.25 mL of deionized water and 0.5 mL of 60 mM trisodium citrate into 13.75 mL of the sample solution. This diluted solution was used as a seed solution to obtain Au NSs of different sizes by controlling the number of repeating steps.

Synthesis of Silver Nanospheres (Ag NSs). Ag NSs were prepared by chemical reduction of silver nitrate using ascorbic acid.[38] Briefly, 10 mg $AgNO_3$ and 30 mg trisodum citrate were dissolved in 50 mL of deionized water. 10, 20, 100, 500, or 1000 μL of 0.1 N NaOH

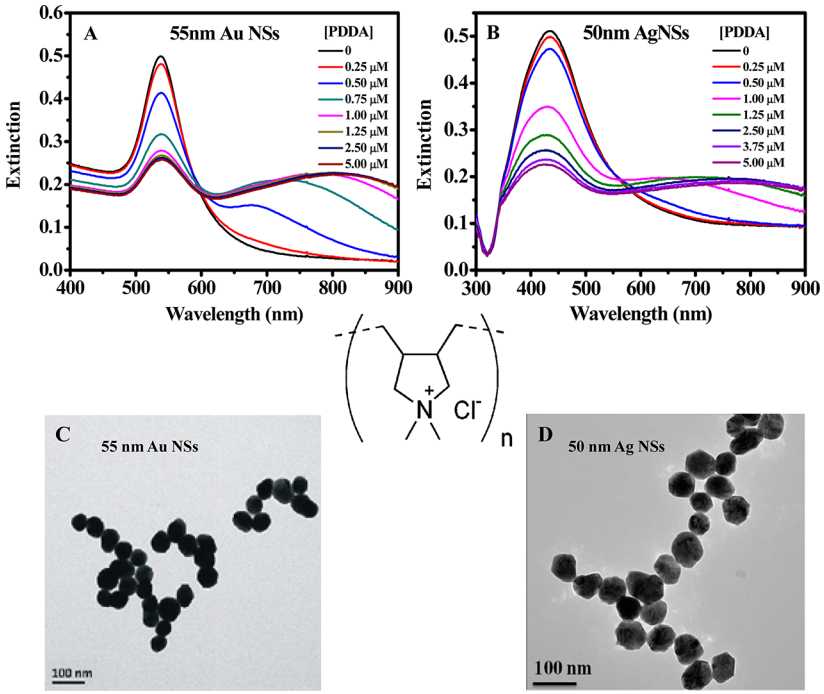

Figure 2. (A, B) UV−vis extinction spectra and (C, D) TEM images of 55-nm Au NSs (panels A and C) and 50-nm Ag NSs (panels B and D) in the presence of 1.25 μM of PDDA; The molecular structure of PDDA is shown in the middle of the figure.

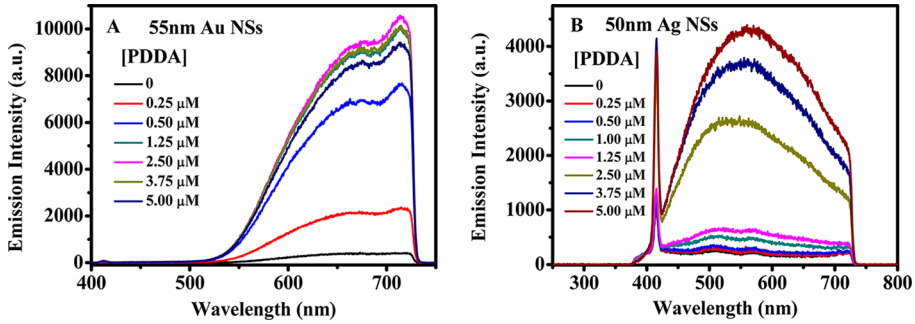

Figure 3. Two-photon excitation photoluminescence spectra of (A) 55-nm Au NSs and (B) 50-nm Ag NSs, in the presence of different amounts of PDDA.

was added under stirring. Ten milliliters (10 mL) of solution containing 20 mg of ascorbic acid was then added dropwise. The mixture solution was stirred for another 1 h to obtain Ag NSs of different sizes.

Instrumentations and Characterizations. Transmission electron microscopy (TEM) images of nanoparticles were taken from a Philips Model CM10 TEM microscope (at an accelerating voltage of 100 kV). Ultraviolet−visible (UV−vis) extinction spectra were measured by using a Shimadzu Model UV-2550 spectrophotometer. The two-photon excitation photoluminescence measurements were performed using an Avesta Model TiF-100 M femtosecond (fs) Ti:sapphire oscillator as the excitation source. The output laser pulses have a central wavelength of 820 nm, with a pulse duration of 80 fs and a repetition rate of 84.5 MHz. The laser beam was focused onto the samples using a lens with a focus length of 3.0 cm. The emission was collected at an angle of 90° to the direction of the excitation beam, to minimize the scattering. The emission signal was directed into a CCD (Princeton Instruments, Model Pixis 100B) coupled monochromator (Acton, Model Spectra Pro 2300i) with an optical fiber. A 750-nm short pass filter was placed before the spectrometer to minimize the scattering from the excitation light.

RESULTS AND DISCUSSION

Au NSs of eight different sizes (average diameters of 20, 30, 40, 55, 80, 95, 110, and 120 nm) and Ag NSs of five different sizes (average diameters of 15, 30, 50, 75, and 100 nm) were prepared to investigate the particle-size-dependent enhancement effects. Their extinction spectra and TEM images are shown in Figure 1. The obtained Au NSs (Figure 1c) are uniform with quasi-spherical shapes. Ag NSs (Figure 1D) have relative broader size distributions. As the particle size increases, the surface plasmon resonance (SPR) band of both Au and Ag NSs gradually shifted to red, accompanied with spectra broadening. The SPR band maximum changed from 523 to 594 nm for Au NSs as the particle size increased from 20 nm to 120 nm, and from 389 nm to 506 nm for Ag NSs as the particle size increased from 15 nm to 100 nm. The shoulder at 400 nm in the extinction spectra of 75- and 100-nm Ag NSs is the characteristic quadrupole SPR mode, which is typical for large-sized nanoparticles.[37,39]

A positively charged polyelectrolyte, PDDA, was employed to induce the coupling of negatively charged metal NPs, which is due to electrostatic interaction. PDDA is a saturated polymer

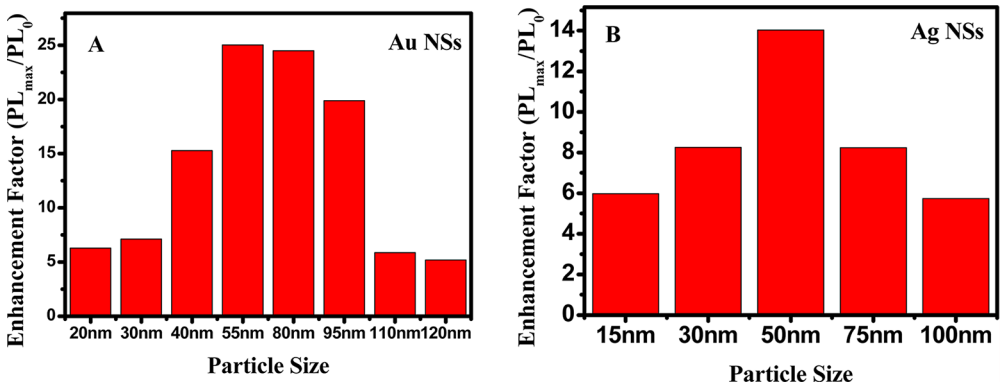

Figure 4. Size-dependent TPPL enhancement factors for (A) coupled Au NSs and (B) coupled Ag NSs.

that has no absorption in the visible to near-IR range, which excludes the possible complications that are due to potential resonant interactions between the metal NPs and polymers. All the nanoparticles were centrifuged to remove the excess sodium citrate then diluted to an extinction maxima of 0.5 before the addition of PDDA. Upon the addition of oppositely charged PDDA, the metal NPs solution rapidly changed the color, indicating the formation of aggregates. The TEM images indicated the formation of chainlike nanoaggregates. All the samples displayed similar trends after the addition of PDDA (see the Supporting Information) and the results of 55-nm Au NSs and 50-nm Ag NSs are presented for illustration purposes (Figure 2). The aggregation was induced by the electrostatic interactions between the negatively charged metal NPs and the positively charged PDDA. The resulted plasmon coupling was confirmed by their extinction spectra (see Figures 2A and 2B). The addition of PDDA resulted in a decrease in the original SPR band of Au and Ag NPs, accompanied by the appearance of a new SPR band at the longer wavelength range. The new SPR band at longer wavelength further shifted to red gradually with the increasing concentration of PDDA. This new SPR band corresponds to the longitudinal SPR mode along the long axis of coupled nanostructures. The further red-shifted longitudinal bands indicate the formation of aggregates with increasing length.

TPPL spectra of Au and Ag NPs before and after the addition of PDDA were measured by using 820-nm fs laser pulses as the excitation source. Figure 3 shows the representative TPPL spectra of 55-nm Au NSs and 50-nm Ag NSs in the presence of different amounts of PDDA. The TPPL spectra of all Au and Ag NPs were rather broad, because of the formation of aggregates with a wide size distribution. The TPPL intensity of the coupled nanoparticles steadily increased upon the gradual addition of PDDA and became saturated as an excess amount of PDDA was added (see Figures S3 and S4 in the Supporting Information). A maximum enhancement of 25-fold was obtained for coupled 55-nm Au NSs and 14-fold for coupled 50-nm Ag NSs. The enhanced TPPL could be explained as a result of increased extinction at the excitation wavelength, as plasmon coupling in the aggregated metal NPs results in the formation of a strong longitudinal band that is resonant with the excitation wavelength. This new longitudinal band provides an intermediate state that greatly promotes two-photon excitation processes.[34] On the other hand, the enhanced local electric field near the excitation wavelength due to plasmon coupling also contributes to the enhanced TPPL. Increasing concentration of PDDA results in the formation of more coupled nanostructures and increased extinction in the near-IR range, consequently enhancing the two-photon absorption efficiency at the excitation wavelength. This is consistent with the previous calculation by Bouhelier et al. that the field enhancement maximum coincides with the plasmon resonance of a gold nanoparticle dimer.[40] In addition to the broad TPPL, a strong sharp peak was also observed at 410 nm in the Ag samples, which is due to enhanced second-harmonic generation (SHG) of the aggregated nanostructures. The enhancement in SHG is much larger in Ag NPs, compared to Au NPs. The enhanced SHG can also be ascribed to an enhanced local field and increased asymmetry after particle coupling. Detailed discussion of the SHG is beyond the scope of this paper and will not be further pursued here.

Figure 4 shows the maximum TPPL enhancement factors versus the particle size for both Au and Ag samples. As the size of isolated nanoparticles increased, the TPPL enhancement factor of coupled nanoparticles increased first and then decreased for both Au and Ag NSs. The optimum size for TPPL enhancement was found to be 55 nm for Au NSs (with a maximum enhancement factor of 25-fold) and 50 nm for Ag NSs (with a maximum enhancement factor of 14-fold). The lower enhancement factor for PDDA-induced Ag nano-aggregates than the previously reported conjugated polymer-induced Ag nanoaggregates[32] is likely due to the different extent of coupling and possible resonant interactions between conjugated polymers and metal NPs. The size-dependent enhancement factor can be understood from two different aspects: first is the size-dependent electric field enhancement; second is the change in extinction at the excitation wavelength (820 nm). It is known that plasmon-induced electric field is size-dependent and will increase for larger nanoparticles for a fixed junction width.[41] In addition, the near fields extend further out from the metal and cause stronger plasmon coupling and larger electric field enhancement, as the size of metal particle increases.[38] However, the particle radiative damping rate increases with particle size, which leads to a large broadening of the plasmon line at the largest nanoparticle sizes studied (as evidenced by the extinction spectra shown in Figures 1A and 1B). The increase of radiation damping implies an increased dephasing of the coupled plasmon mode and thus tends to decrease the local field enhancement in the space between the particles.[42] The electric field and TPPL enhancement factor are thus expected to first increase with the particle size and then decrease for very large metal nanoparticles. On the other hand, as the particle size increases, the coupled nanoparticles show a larger increase at the excitation wave-

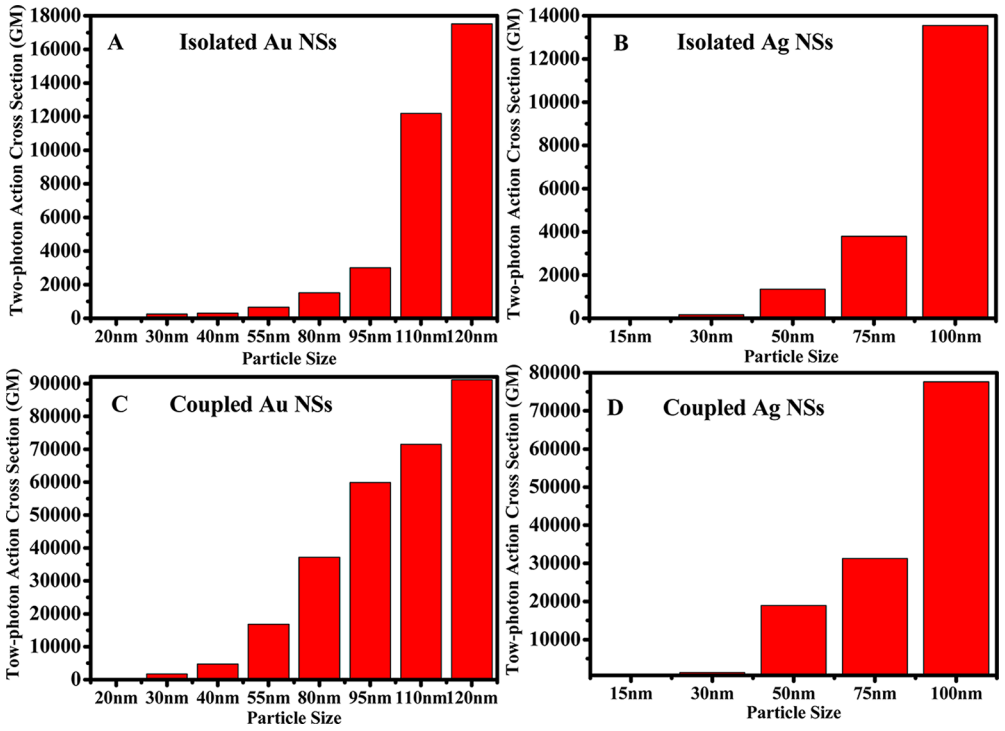

Figure 5. Size-dependent two-photon action cross-section of (A) isolated Au NSs and (B) isolated Ag NSs, as well as (C) coupled Au NSs and (D) coupled Ag NSs.

length, which provides more intermediate states to promote two-photon excitation processes. However, if the particle size is too big, the tail of the plasmon resonance of isolated nanoparticles starts to overlap with the excitation wavelength; consequently, the isolated nanoparticles themselves starts to display strong TPPL background (see Figures 5A and 5B), resulting in reduced enhancement factors in the coupled nanostructures.

The aggregation-induced TPPL enhancement could be utilized in two-photon excitation imaging and sensing.[34] Two-photon excitation-based applications have many unique advantages, such as three-dimensional (3D) selectivity, reduced photobleaching, and deep penetration into biological tissues. The wide applications of these techniques require high brightness under two-photon excitation. TPPL brightness is generally quantitatively characterized by two-photon action cross section (φ_{2p}= σ_{2p} × η), where σ_{2p} is the two-photon absorption cross section and η is the emission quantum efficiency. The applications of two-photon techniques have been limited by the small two-photon action cross sections of small organic molecules. The two-photon action cross section of these coupled metal nanoparticles was calculated using Au nanorods with an aspect ratio of 4 (φ_{2p} = 30 000 GM at 820 nm) as the reference.[43] [Note: 1 GM = 10^{-50} cm^4 s/photon.] Both isolated and coupled Au and Ag NPs exhibited increasing φ_{2p} values with the increasing particle sizes, as shown in Figure 5. The two-photon action cross section of isolated 120-nm Au NSs and 100-nm Ag NSs were determined to be 1.8 × 10^4 and 1.4 × 10^4 per particle, comparable to that of Au nanorods. The two-photon action cross section of coupled 120-nm Au NSs and 100-nm Ag NSs reached up to 9.1 × 10^4 and 7.8 × 10^4 per NS. Considering that the formed nanoaggregates have a wide distribution of different sizes and structures, the optimum structures are expected to have even larger two-photon action cross sections, which will motivate us to search for nanostructures with extremely high two-photon absorption cross sections and explores their potential applications. The huge two-photon action cross sections of aggregated metal nanostructures are expected to open many new pathways for developing two-photon-based applications.

In summary, the two-photon excitation photoluminescence (TPPL) of Au and Ag NSs was found to be significantly enhanced upon coupling induced by PDDA. The TPPL enhancement factors were determined to increase first and then decrease as the particle size increased for both Au and Ag NPs. The highest TPPL enhancement was obtained for coupled 55-nm Au NSs and 50-nm Ag NSs, with enhancement factors of 25- and 14-fold, respectively. The coupled Au and Ag NPs displayed two-photon action cross sections of up to 9 × 10^4 GM per particle. Similar to Ag nanoparticles, Au NPs also displayed large coupling induced TPPL enhancement. Considering their excellent biocompatibility, high inertness, and easy preparation, Au NPs are expected to find many new applications in two-photon biosensing and bioimaging to fully take unique advantage of the two-photon excitation.

■ ASSOCIATED CONTENT

Ⓢ Supporting Information

UV−vis extinction and TPPL spectra of coupled Au and Ag nanospheres; the method and procedure of calculating their two-photon action cross sections using Au NRs as the reference. This information is available free of charge via the Internet at http://pubs.acs.org.

■ AUTHOR INFORMATION

Corresponding Author

*E-mail: chmxqh@nus.edu.sg.

Author Contributions

§These authors contributed equally to this work.

Notes

The authors declare no competing financial interest.

■ ACKNOWLEDGMENTS

We thank the financial support from DSTA Singapore (Project No. DSTA-NUS-DIRP/9010100347), the Singapore-MIT Alliance of Research and Technology (SMART) program under National Research Foundation Singapore and the Economic Development Board (SPORE, No. COY-15-EWI-RCFSA/N197-1).

■ REFERENCES

(1) Saha, K.; Agasti, S. S.; Kim, C.; Li, X.; Rotello, V. M. *Chem. Rev.* **2012**, *112*, 2739−2779.
(2) Jiang, Y.; Horimoto, N. N.; Imura, K.; Okamoto, H.; Matsui, K.; Shigemoto, R. *Adv. Mater.* **2009**, *21*, 2309−2313.
(3) Polavarapu, L.; Manna, M.; Xu, Q.-H. *Nanoscale* **2011**, *3*, 429−434.
(4) Shang, L.; Dorlich, R. M.; Brandholt, S.; Schneider, R.; Trouillet, V.; Bruns, M.; Gerthsen, D.; Nienhaus, G. U. *Nanoscale* **2011**, *3*, 2009−2014.
(5) Tong, L.; Cobley, C. M.; Chen, J.; Xia, Y.; Cheng, J.-X. *Angew. Chem., Int. Ed.* **2010**, *49*, 3485−3488.
(6) Griffin, J.; Singh, A. K.; Senapati, D.; Lee, E.; Gaylor, K.; Jones-Boone, J.; Ray, P. C. *Small* **2009**, *5*, 839−845.
(7) Jin, R.; Jureller, J. E.; Kim, H. Y.; Scherer, N. F. *J. Am. Chem. Soc.* **2005**, *127*, 12482−12483.
(8) Lee, Y. H.; Yan, Y.; Polavarapu, L.; Xu, Q.-H. *Appl. Phys. Lett.* **2009**, *95*, 023105.
(9) Wang, F. X.; Rodríguez, F. J.; Albers, W. M.; Ahorinta, R.; Sipe, J. E.; Kauranen, M. *Phys. Rev. B* **2009**, *80*, 233402.
(10) Chen, H.; Ming, T.; Zhao, L.; Wang, F.; Sun, L.-D.; Wang, J.; Yan, C.-H. *Nano Today* **2010**, *5*, 494−505.
(11) Ehrenreich, H.; Philipp, H. R. *Phys. Rev.* **1962**, *128*, 1622−1629.
(12) Noguez, C. *J. Phys. Chem. C* **2007**, *111*, 3806−3819.
(13) Yeshchenko, O. A.; Dmitruk, I. M.; Alexeenko, A. A.; Losytskyy, M. Y.; Kotko, A. V.; Pinchuk, A. O. *Phys. Rev. B* **2009**, *79*, 235438.
(14) Zheng, Y. B.; Kiraly, B.; Cheunkar, S.; Huang, T. J.; Weiss, P. S. *Nano Lett.* **2011**, *11*, 2061−2065.
(15) Nie, S.; Emory, S. R. *Science* **1997**, *275*, 1102−1106.
(16) Bardhan, R.; Grady, N. K.; Cole, J. R.; Joshi, A.; Halas, N. J. *ACS Nano* **2009**, *3*, 744−752.
(17) Butet, J.; Russier-Antoine, I.; Jonin, C.; Lascoux, N.; Benichou, E.; Brevet, P.-F. *Nano Lett.* **2012**, *12*, 1697−1701.
(18) Fang, Z.; Fan, L.; Lin, C.; Zhang, D.; Meixner, A. J.; Zhu, X. *Nano Lett.* **2011**, *11*, 1676−1680.
(19) Imura, K.; Nagahara, T.; Okamoto, H. *J. Am. Chem. Soc.* **2004**, *126*, 12730−12731.
(20) Mohamed, M. B.; Volkov, V.; Link, S.; El-Sayed, M. A. *Chem. Phys. Lett.* **2000**, *317*, 517−523.
(21) Mühlschlegel, P.; Eisler, H.-J.; Martin, O. J. F.; Hecht, B.; Pohl, D. W. *Science* **2005**, *308*, 1607−1609.
(22) Polavarapu, L.; Xu, Q.-H. *Langmuir* **2008**, *24*, 10608−10611.
(23) Ueno, K.; Juodkazis, S.; Mizeikis, V.; Sasaki, K.; Misawa, H. *Adv. Mater.* **2008**, *20*, 26−30.
(24) Varnavski, O. P.; Mohamed, M. B.; El-Sayed, M. A.; Goodson, T., III *J. Phys. Chem. B* **2003**, *107*, 3101−3104.
(25) Zhang, Y.; Grady, N. K.; Ayala-Orozco, C.; Halas, N. J. *Nano Lett.* **2011**, *11*, 5519−5523.
(26) Kim, H. M.; Cho, B. R. *Chem.−Asian J.* **2011**, *6*, 58−69.
(27) Narayanan, A.; Varnavski, O.; Mongin, O.; Majoral, J.-P.; Blanchard-Desce, M.; Goodson, T., III. *Nanotechnology* **2008**, *19*, 115502.
(28) Narayanan, A.; Varnavski, O. P.; Swager, T. M.; Goodson, T., III. *J. Phys. Chem. C* **2008**, *112*, 881−884.
(29) Beversluis, M. R.; Bouhelier, A.; Novotny, L. *Phys. Rev. B* **2003**, *68*, 115433.
(30) Imura, K.; Nagahara, T.; Okamoto, H. *J. Phys. Chem. B* **2005**, *109*, 13214−13220.
(31) Dulkeith, E.; Niedereichholz, T.; Klar, T. A.; Feldmann, J.; von Plessen, G.; Gittins, D. I.; Mayya, K. S.; Caruso, F. *Phys. Rev. B* **2004**, *70*, 205424.
(32) Guan, Z.; Polavarapu, L.; Xu, Q.-H. *Langmuir* **2010**, *26*, 18020−18023.
(33) Wang, H.; Huff, T. B.; Zweifel, D. A.; He, W.; Low, P. S.; Wei, A.; Cheng, J.-X. *Proc. Natl. Acad. Sci. U.S.A.* **2005**, *102*, 15752−15756.
(34) Jiang, C.; Guan, Z.; Lim, S. Y. R.; Polavarapu, L.; Xu, Q.-H. *Nanoscale* **2011**, *3*, 3316−3320.
(35) Jain, P. K.; Huang, W.; El-Sayed, M. A. *Nano Lett.* **2007**, *7*, 2080−2088.
(36) Ringe, E.; McMahon, J. M.; Sohn, K.; Cobley, C.; Xia, Y.; Huang, J.; Schatz, G. C.; Marks, L. D.; Van Duyne, R. P. *J. Phys. Chem. C* **2010**, *114*, 12511−12516.
(37) Bastús, N. G.; Comenge, J.; Puntes, V. *Langmuir* **2011**, *27*, 11098−11105.
(38) Zhang, J.; Fu, Y.; Chowdhury, M. H.; Lakowicz, J. R. *J. Phys. Chem. C* **2007**, *112*, 18−26.
(39) Rodríguez-Fernández, J.; Pérez-Juste, J.; García de Abajo, F. J.; Liz-Marzán, L. M. *Langmuir* **2006**, *22*, 7007−7010.
(40) Bouhelier, A.; Bachelot, R.; Lerondel, G.; Kostcheev, S.; Royer, P.; Wiederrecht, G. P. *Phys. Rev. Lett.* **2005**, *95*, 267405.
(41) Marinica, D. C.; Kazansky, A. K.; Nordlander, P.; Aizpurua, J.; Borisov, A. G. *Nano Lett.* **2012**, *12*, 1333−1339.
(42) Dahmen, C.; Schmidt, B.; von Plessen, G. *Nano Lett.* **2007**, *7*, 318−322.
(43) Zijlstra, P.; Chon, J. W. M.; Gu, M. *Nature* **2009**, *459*, 410−413.